Research Article

Journal of Molecular Recognition

Received: 18 October 2013, Revised: 20 December 2013, Accepted: 21 December 2013, Published online in Wiley Online Library

(wileyonlinelibrary.com) DOI: 10.1002/jmr.2354

Dynamic and geometric analyses of *Nudaurelia capensis* ω virus maturation reveal the energy landscape of particle transitions

Jinghua Tang[a], Bradley M. Kearney[b], Qiu Wang[c], Peter C. Doerschuk[c], Timothy S. Baker[a] and John E. Johnson[b]*

Quasi-equivalent viruses that infect animals and bacteria require a maturation process in which particles transition from initially assembled procapsids to infectious virions. *Nudaurelia capensis* ω virus (NωV) is a *T* = 4, eukaryotic, single-stranded ribonucleic acid virus that has proved to be an excellent model system for studying the mechanisms of viral maturation. Structures of NωV procapsids (diameter = 480 Å), a maturation intermediate (410 Å), and the mature virion (410 Å) were determined by electron cryo-microscopy and three-dimensional image reconstruction (cryoEM). The cryoEM density for each particle type was analyzed with a recently developed maximum likelihood variance (MLV) method for characterizing microstates occupied in the ensemble of particles used for the reconstructions. The procapsid and the mature capsid had overall low variance (*i.e.*, uniform particle populations) while the maturation intermediate (that had not undergone post-assembly autocatalytic cleavage) had roughly two to four times the variance of the first two particles. Without maturation cleavage, the particles assume a variety of microstates, as the frustrated subunits cannot reach a minimum energy configuration. Geometric analyses of subunit coordinates provided a quantitative description of the particle reorganization during maturation. Superposition of the four quasi-equivalent subunits in the procapsid had an average root mean square deviation (RMSD) of 3 Å while the mature particle had an RMSD of 11 Å, showing that the subunits differentiate from near equivalent environments in the procapsid to strikingly non-equivalent environments during maturation. Autocatalytic cleavage is clearly required for the reorganized mature particle to reach the minimum energy state required for stability and infectivity. Copyright © 2014 John Wiley & Sons, Ltd.

Keywords: autocatalysis; cryoEM; virus maturation; virus capsid quasi-equivalence; maximum likelihood estimation; variance map; NωV; virus particle dynamics

INTRODUCTION

Virus maturation is the process by which a particle transitions from a fragile, non-infectious procapsid to a robust, infectious virion. This process is observed universally in animal viruses and bacteriophage and is a target for antiviral development (Salzwedel *et al*., 2007). *Nudaurelia capensis* ω virus (NωV) is an exceptionally accessible system for the study of virus maturation, and we use it here to characterize the details of conformational changes associated with particle transitions as well as the dynamic character of individual intermediates.

N. capensis ω virus is a *T* = 4, icosahedral insect virus with a bi partite, positive-sense ribonucleic acid genome. Procapsids of NωV are fragile, round, and porous with a diameter of 480 Å. They are comprised of 240 copies of a 644-amino-acid capsid protein subunit. Procapsids can be made by expressing the capsid protein gene in a baculovirus system and purifying particles at neutral pH (Agrawal and Johnson, 1995). NωV is valuable for investigating the conversion from procapsid to capsid because lowering the pH to 5.0 triggers the transition that results in a 410-Å diameter capsid. The full length subunit, α, undergoes an autolytic cleavage, with a half-life of 30 min, that begins immediately following capsid formation and occurs between residues N570 and F571, creating the β protein (1–570) and the γ peptide (571–644). The γ peptides remain associated with the capsid in a non-covalent manner. Auto-proteolysis induces changes that result in a more robust virus particle that does not expand when the pH is raised. A mutant form of NωV (N570T, hereafter referred to as "NT") forms 480-Å diameter NT procapsids and converts to 410-Å NT capsids at pH 5. NT is unable to undergo auto-proteolysis and will revert to the 480-Å form upon restoring to neutral pH (Taylor *et al*., 2002).

The formation of an infectious virus must overcome two apparently conflicting biophysical principles: reversibility and stability. Most intracellular protein complexes marginally favor assembly over disassembly as this produces a self-correcting and accurate association process as well as marginal stability that are appropriate for their transient existence. However, viruses must survive harsh, extracellular environments that

* *Correspondence to: John E. Johnson, Department of Integrative Structural and Computational Biology, The Scripps Research Institute, La Jolla, CA 92037, USA. E-mail: jackj@scripps.edu*

a *J. Tang, T. S. Baker*
Department of Chemistry and Biochemistry, and Division of Biological Sciences, University of California, San Diego, La Jolla, CA, 92093-0378, USA

b *B. M. Kearney, J. E. Johnson*
Department of Integrative Structural and Computational Biology, The Scripps Research Institute, La Jolla, CA, 92037, USA

c *Q. Wang, P. C. Doerschuk*
Department of Biomedical Engineering, School of Electrical and Computer Engineering, Cornell University, 135 Weill Hall, Ithaca, NY, 14853-6007, USA

would disintegrate particles made with reversible interactions. If initial subunit interactions were strong enough to produce a robust particle, they would be unable to self-correct, and kinetic traps would inhibit accurate particle formation (Zlotnick and Mukhopadhyay, 2011). The solution that provides flexibility for proper assembly and stability in the virus results from a staged association process (*i.e.*, maturation). Nearly reversible interactions of protein subunits initially form a procapsid with subunits properly positioned, and this is followed by a chemically encoded transition to a robust virus particle.

NT procapsid, NT capsid, and wild type (WT) capsid structures were previously determined at resolutions of 8, 6, and 6 Å, respectively, by electron cryo-microscopy (cryoEM) (Tang *et al*., 2009). Subunit environments in these particles were quantitatively analyzed by fitting an atomic model (Tang *et al*., 2009) to the 8-Å cryoEM reconstruction of the procapsid and by analyzing the X-ray model of the WT capsid. Here we show that superposition of the quasi-equivalent (Caspar and Klug, 1962) procapsid subunits by rigid body rotations, with quasi-symmetry axes passing through the center of the particle, yields an overall atom root mean square deviation (RMSD) of 3 Å. Icosahedral symmetry relates asymmetric units in the capsid with zero RMSD. Thus, quasi-symmetry relates subunits in the procapsid with nearly the same RMSD as icosahedral symmetry indicating closely similar, quasi-symmetric environments. We then performed dynamic analysis of the procapsid cryoEM images using a maximum likelihood variance (MLV) method (Wang *et al*., 2013), and this revealed that the entire particle had nearly the same, moderately low variance, consistent with the homogeneous subunit environments. A maturation intermediate (mimicked by the NT capsid that has not undergone autocatalytic cleavage) and the fully mature particle (WT capsid) are structurally indistinguishable at pH 5 at 6-Å resolution. Geometric analyses of these particles revealed breakdown of quasi-equivalence, as average atom RMSD values were 11.4 Å. MLV analysis showed that the variance of the mature particle was, on average, one fourth to one half of that of the NT intermediate. This observation demonstrates that, at pH 5, NT capsid is a metastable particle with sufficient stored energy to drive the autocatalysis associated with the final stage of maturation.

MATERIALS AND METHODS

Geometric comparison of subunit environments in the procapsid and capsid

The crystal structure of the mature virion (PDB code: 1OHF) was fitted previously to the NT procapsid and WT capsid cryoEM density maps (Tang *et al*., 2009). A subset of the atomic coordinates (residues 124–530) corresponding just to the core jellyroll motif and the Ig-like domain were selected for analyzing the quasi-equivalence of the neighboring subunits in the fitted models. The rotation matrices that minimized the RMSD of the quasi-equivalent subunits were computed in two different ways. The first method (Method 1) measured the deviation of the particle from a sphere by constraining the rotation axes of the quasi-symmetry elements that minimized the backbone RMSD, to pass through the center of the particle. The second method (Method 2) minimized the RMSD values between quasi-equivalent subunits in a manner comparable to that achieved by modern protein super positioning algorithms such as incorporated into LSQMAN (Kleywegt, 1996) or as devised by McLachlan (McLachlan, 1982). This approach implicitly allows for translation by placing no constraints on the direction and location of the quasi-symmetry axes (*i.e.*, this allows six degrees of freedom). The RMSD values for all super positions are closely similar, deviating only by differences in the tertiary structures of the four independent subunits (ranging from 0.4 to 1.5 Å). With Method 2, quasi-equivalence is analyzed not by RMSD but by comparing the orientations and positions of the axes that relate the subunits.

Variance map calculations

We used cryoEM images from three previously recorded NωV data sets (Tang *et al*., 2009) to generate structures and variance maps with the MLV program. The reconstructions closely resemble the reported structures, albeit at lower resolution (22 Å for both the NT procapsid and capsid, and 15 Å for the WT capsid) owing to the computational demand of the MLV algorithm that restricted both the number of images used during reconstruction and the number of icosahedral harmonics (Wang *et al*., 2013). Briefly, the three-dimensional electron scattering density is represented as a weighted sum of basis functions. Instead of treating the weights as numbers and estimating the numbers from the image data, the weights are treated as Gaussian random variables and the means and covariance of the weights are estimated from the image data. The maximum likelihood estimator is computed by an expectation-maximization algorithm. From the means and covariance values of the weights, the space-varying mean and the space-varying variance of the electron scattering density can both be computed at every voxel in the reconstructed density map. The space-varying mean is the nominal reconstruction, and the space-varying variance (or its square root, which is the space-varying standard deviation) describes the heterogeneity of the particle ensemble. To understand how conformational flexibility is distributed within each subunit, the flexibility (quantified as variance) was determined at each amino acid residue of the X-ray model. Specifically, the variance at voxels within 10 Å of the C-alpha carbon of the amino acid residue was averaged, and the average is the variance value assigned to that residue. The standard deviation (square root of the variance) was computed, scaled to the range of 25–45, and put into the B-factor column in the subunit coordinate file from which Figures 3 and 4 were computed. The variance maps from the different data sets were placed on the same overall scale with the following procedure. Each reconstruction was scaled to the WT capsid reconstruction by determining a gain, which minimizes the integrated absolute value of the difference map as described (Wang *et al*., 2013). The variance map corresponding to that reconstruction was then scaled by the square of the gain in order to place all variance maps on the same scale. Chimera (Pettersen *et al*., 2004) was used to render the variances from low to high using a blue to red rainbow color scheme.

RESULTS

Three particle types were isolated: NT procapsid, which corresponds to the initial assembly product; NT capsid, which corresponds to the intermediate prior to autocatalytic cleavage; and WT capsid, which is the fully mature particle. NT procapsid and WT capsid were each analyzed by Methods 1 and 2 to quantitate the similarity of their quasi-equivalent environments. With respect to this analysis, NT capsid is indistinguishable from WT capsid. Variance maps were also computed for all three particle types to quantitate their dynamic character. In contrast to temperature factors computed with X-ray crystallographic data that reflect atomic motion at angstrom resolution, the variance plotted on the voxel arrays presented here corresponds to an

average occupancy. Thus, the variance describes the number and extent of microstates sampled by the particles as projected in the entire image collection.

The $T = 4$ surface lattice of NωV has quasi-3-folds, quasi-6-folds, and also two different quasi-2-fold axes that, together, provide a convenient way to compare the fidelity of subunit super positions (Figure 1A). These relationships correspond to only six unique pairwise subunit super positions because of the combination of quasi and icosahedral symmetry operations. In our analysis below, we chose to highlight a specific set of super positions that emphasize the molecular switching required to form an icosahedral-shaped particle in the compact capsid, but the relationships can also be described in other ways. In the compact, faceted capsid, the quasi-2-fold axes correspond to a "flat" interaction between trimers A1, B1, C1 and D1, D7, D9, and a "bent" interaction between trimers A1, B1, and C1 and A5, B5, and C5 (Figure 1A). Hereafter, in our geometric description, we refer to these quasi-2-fold axes as "flat" and "bent", although, as described below, they are nearly equivalent in the procapsid.

NT procapsid

By choosing quasi-symmetry axes that are constrained to pass through the center of the particle, Method 1 shows (Table 1) that when superimposing subunits related by the quasi-3-fold symmetry element, A1 on B1 (blue and red) has an RMSD of 3.64 Å, B1 on C1 (red and green) has an RMSD of 2.11 Å, and C1 on A1 (green and blue) has an RMSD of 4.34 Å. When superimposed by the adjacent quasi-2-fold symmetry element at the "flat" contact (Figure 1) between subunits C1 and D1 (green and yellow, respectively), the RMSD is 1.33 Å. The same operator relates subunits B1 and D7 (red and yellow) with an RMSD of 2.69 Å and A1 and D9 (blue and yellow) with an RMSD of 4.36 Å. Overall, the small RMSD values produced by Method 1 demonstrate that the quasi-symmetry relationships are nearly as precise as the perfect icosahedral symmetry relationships, which implies that there is exceptional similarity in the subunit environments. Furthermore, the procapsid geometry is consistent with the spherical shape approximation (*i.e.*, the subunits all lie at approximately the same radius and in the same orientation with respect to the particle center) that is imposed by forcing quasi-symmetry axes to pass through the center of the particle. Allowing six degrees of freedom to superimpose the subunits in the NT capsid in Method 2 does little to improve the RMSD values or change the orientation of the axes (Table 2).

The uniformity of the variance in the protein shell portion of the NT procapsid structure (Figure 2A, B) is striking yet consistent with the similar environments of all four classes of subunit. The relatively low value of the variance reflects minimum variation in the particle ensemble at the moment of flash freezing at neutral pH. This is further emphasized when the variance is plotted onto the tertiary structures of the individual subunit atomic models that were fitted into the procapsid density map (Figure 3A).

NT and WT capsids

We used the 2.8-Å X-ray atomic coordinates of 1OHF (Helgstrand *et al.*, 2004) to perform geometric analysis of the capsid form of NωV. Given that these coordinates fit into the WT (cleaved) and NT (uncleaved) capsid cryoEM density maps with no significant variation from the crystal structure, only the X-ray coordinates were analyzed with Methods 1 and 2. The RMSD values for the

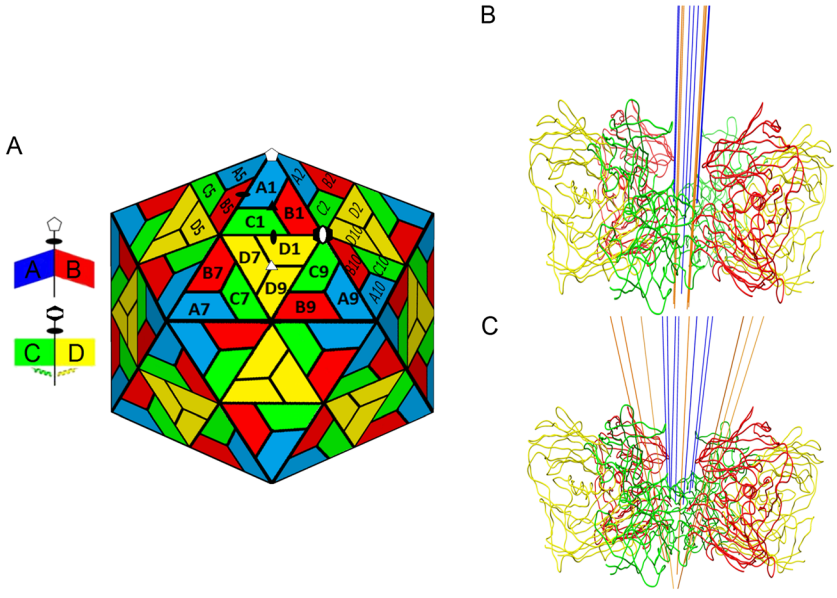

Figure 1. Diagram of NωV WT capsid and rotation axes derived for the two methods of quasi-symmetry analysis. (A) Color-coded schematic representation of the NωV capsid. Dimer interfaces at the quasi-2-fold axes occur with either bent (A–B) or flat (C–D) conformations. White symbols identify icosahedral symmetry axes, and black symbols identify quasi-2-fold (ellipses) and quasi-3-fold (triangle) axes. The hexagon with the white ellipsis embedded identifies a quasi-6-fold symmetry axis (icosahedral 2-fold axis). (B) Method 1: RMSD minimized solely by rotations (three degrees of freedom). The axes relating subunits in the procapsid (blue lines) and capsid (orange lines) are shown with a cartoon representation of the subunits at a quasi-6-fold axis. Subunits are colored according to Figure 1A.The orientations of the rotation axes are very similar, differing only by 3°. The axes that minimize the RMSD are roughly the same, but there are large differences in the RMSD value when comparing the same operator in the procapsid and capsid (Table 1). (C) Method 2: Translation allowed in minimization of RMSD (six degrees of freedom). While the rotation axes in the procapsid retain similar orientations to Method 1, the directions of the axes differ significantly in the capsid demonstrating a large deviation from a spherical subunit distribution in the mature particle.

Table 1. Restricted symmetry axis orientations and rotations that minimize the RMSD between quasi-equivalent subunits

Subunits	Axis	Procapsid					Capsid				
		Rotation angle (deg)	RMSD (Å) [a]	Rotation axis angles (deg) [b]			Rotation angle (deg)	RMSD (Å) [a]	Rotation axis angles (deg) [b]		
				x	*y*	*z* [c]			*x*	*y*	*z* [c]
Quasi-equavalent axes											
A1–B1	3-fold	115.4	3.6	78.8	73.4	20.3	113.1	13.5	78.8	74.5	19.3
B1–C1	3-fold	126.2	2.1	79.2	72.6	20.6	128.4	10.1	78.9	74.2	19.6
C1–A1	3-fold	118.3	4.3	79.6	73.3	19.8	105.8	14.7	78.2	74.0	19.9
C1–D1	2-fold	178.8	1.3	74.2	81.4	18.0	173.0	6.9	74.0	82.1	17.8
B1–D7	2-fold	175.2	2.7	73.3	81.0	19.1	174.5	9.1	73.7	82.0	18.4
A1–D9	2-fold	179.7	4.4	74.2	81.7	18.0	177.6	16.8	73.4	82.2	18.6
Icosahedral controls											
B1–B10	2-fold	180.0	0.0	60.1	72.0	35.9	180.0	0.0	60.0	72.0	36.0
D1–D7	3-fold	120.0	0.0	69.1	90.0	20.9	120.0	0.0	69.1	90.0	20.9
A1–A5	5-fold	72.0	0.0	90.0	58.3	31.7	72.0	0.0	90.0	58.3	31.7

[a]RMSDs in Method 1 discerns the deviation of the subunits from a sphere (*i.e.*, subunit centers are at the same radius from the center of the particle).
[b]Symmetry axes are forced to pass through the center of the paricle.
[c]Coordinates are in the VIPERdb format which is in the icosahedral convention: 2-fold(*z*-axis),3-fold,5-fold,(*x*-axis)2-fold.
There are six unique relationships among the four subunits in a $T=4$ quasi-equivalent surface lattice as shown in Figure 1. RMSD values are computed for the superposition of A1–B1, A1–C1, B1–C1, C1–D1, B1–D7, and A1–D9. Additional relationships are equivalent by icosahedral symmetry although the orientation and rotation angle for the axes relating them are different. For example, when A1 is superimposed on B5 with the quasi-2-fold axis, we get an identical RMSD value as obtained for A1 on B1 related by the quasi-3-fold axis because B1 and B5 are related by the icosahedral 5-fold axis. The metric of interest in this method is the RMSD value of quasi-equivalent subunits.

Table 2. Unrestricted symmetry axis orientations and rotations that minimize the RMSD between quasi-equivalent subunits

Subunits	Axis	Procapsid						Capsid						Angle between axes (deg)
		Rotation angle (deg)	Method 2 RMSD (Å) [a]	Method 1 RMSD (Å)	Rotation axis angles (deg)[b]			Rotation angle (deg)	Method 2	Method 1	Rotation axis angles (deg)[b]			
					x	*y*	*z*[c]		RMSD (Å)[a]	RMSD (Å)	*x*	*y*	*z*	
Quasi-equavalent axes														
A1–B1	3-fold	114.3	0.4	3.6	75.0	75.9	20.8	119.3	0.4	13.5	69.6	89.6	20.4	14.5
B1–C1	3-fold	126.6	1.5	2.1	77.6	72.2	21.9	122.0	1.5	10.1	70.2	88.6	19.9	17.7
C1–A1	3-fold	119.3	1.4	4.3	79.5	75.9	17.6	118.7	1.4	14.7	70.7	89.6	19.3	16.0
C1–D1	2-fold	179.8	0.5	1.3	73.7	83.5	17.6	179.7	0.5	6.9	69.3	89.8	20.8	7.7
B1–D7	2-fold	174.5	1.3	2.7	70.4	80.2	22.0	178.3	1.3	9.1	69.5	88.7	20.6	8.6
A1–D9	2-fold	178.9	1.3	4.4	74.8	83.1	16.9	178.9	1.3	16.8	70.2	90.3	19.8	7.9
Icosahedral controls														
B1–B10	2-fold	180.0	0.0	0.0	60.1	72.0	35.9	180.0	0.0	0.0	60.1	72.0	36.0	0.0
D1–D7	3-fold	120.0	0.0	0.0	69.1	90.0	20.9	120.0	0.0	0.0	69.1	90.0	20.9	0.0
A1–A5	5-fold	72.0	0.0	0.0	90.0	58.3	31.7	72.0	0.0	0.0	90.0	58.3	31.7	0.0

[a]RMSDs in Method 2 discerns the differences in tertiary structure between subunits and are the same between procapsid and capsid.
[b]Symmetry axes are free to take any orientation and position to minimize the RMSD.
[c]Coordinates are in the VIPERdb format which is in the icosahedral convention: 2-fold(*z*-axis),3-fold,5-fold,(*x*-axis)2-fold.
There are six unique relationships among the four subunits in a $T=4$ quasi-equivalent surface lattice as shown in Figure 1. RMSD values are computed for the superposition of A1–B1, A1–C1, B1–C1, C1–D1, B1–D7, and A1–D9. Additional relationships are equivalent by icosahedral symmetry although the orientation and rotation angle for the axes relating them are different. For example, when A1 is superimposed on B5 with the quasi-2-fold axis, we get an identical RMSD value as obtained for A1 on B1 related by the quasi-3-fold axis because B1 and B5 are related by the icosahedral 5-fold axis. The metric of interest in this method is the orientation and rotation of the axes that minimizes the RMSD.

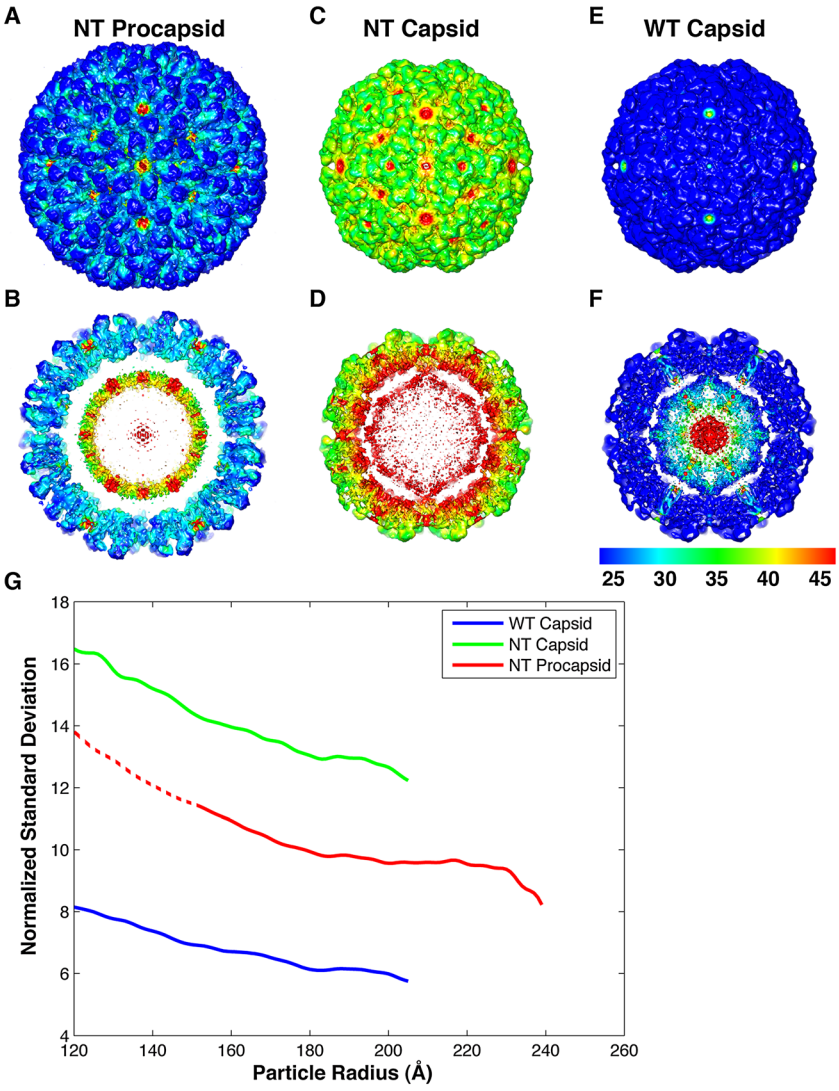

Figure 2. The structural fluctuations of the NωV particles plotted as standard deviation maps corresponding to the square root of the variance with units of electron scattering density. The resolution of the standard deviation maps is ~22 Å for NT procapsid, ~22 Å for NT capsid, and ~15 Å for WT capsid. Panels A, C, and E are surface views of the cryoEM density maps of the NT procapsid, NT capsid, and WT mature capsid, viewed along an icosahedral 2-fold axis of symmetry and color coded according to values of their normalized standard deviation. The non-cleaving NT capsid and the mature cleaved WT capsid exhibit the highest and lowest standard deviations, respectively, and the NT procapsid is intermediate to these two. Panels B, D, and F are the same as A, C, and E but with the front halves of the density maps removed to reveal the standard deviation values for the internal features of the three particles. (G) Plots of the distribution of standard deviation, now normalized to the nominal reconstruction, as a function of radius for each NωV particle. Colored solid portions of the plots correspond to the shell regions of the particles.

subunits corresponding to those in the capsid as generated by Method 1 were C1–D1, 6.9 Å; B1–D7, 9.1 Å; A1–D9, 16.8 Å; A1–B5, 13.5 Å; A5–C1, 14.8 Å; and B1–C1, 10.1 Å. The icosahedral shape of the capsid is inconsistent with the spherical approximation imposed in Method 1, and this is strikingly demonstrated by the large RMSD values that reflect quasi-equivalent environments that have differentiated dramatically from what they are in the procapsid. Method 2 provides a description of the geometric reorganization of the particle (Table 2). The low RMSD values demonstrate that there are only slight differences among the tertiary structures of the four subunits, and the six degrees of freedom used to carry out the super positions via Method 2 reveals the details of the differentiation of subunit environments required to form the new quaternary structure.

The variance maps of NT capsid and WT capsid based on their respective cryoEM reconstructions differ significantly (Figure 2), which is in stark contrast to the indistinguishable nature of these densities when fitting the X-ray coordinates. The variance for the NT capsid is, on average, two to four times that of the WT capsid, which means that the NT capsid samples a much larger range of microstates. The variances for the NT and WT capsids, when plotted on the X-ray models fitted to the respective density maps, clearly illustrate their differences (Figure 3B, C). WT capsid (Figure 3C) displays the same uniform variance as does procapsid (Figure 3A) but with even lower overall values. The NT capsid (Figure 3B) exhibits extremely high variance in the internal helical domain in all four subunits, where the autocatalytic cleavage site is located. Although the variance of the jellyroll and Ig domains in the NT capsid is lower than that in the internal helical domains, it is still exceptionally high when compared to the same domains in the procapsid and WT capsid.

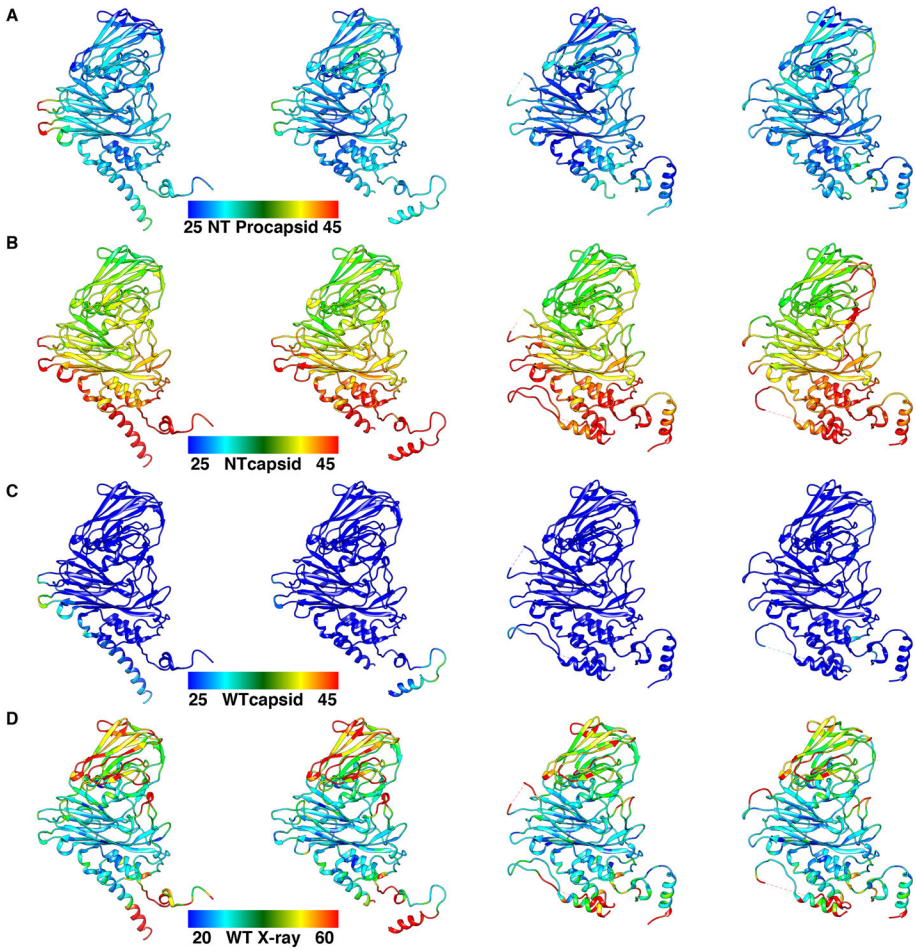

Figure 3. Standard deviations of structural fluctuations (*i.e.*, square root of the variance) within individual subunits. (A) Standard deviation in each of the four quasi-equivalent subunits of the NT procapsid (subunits A, B, C, and D arranged left to right) color coded as pseudo-B factors ranging between 25 and 45. (B) Same as panel A but for the NT capsid. (C) Same as panel A but for the WT capsid. (D) Same as panel A but for the WT X-ray crystal structure and depicted on an absolute B factor scale that ranges between 20 and 60 Å^2.

The extremely high variance of the internal helical domains of NT capsid strongly suggests that structural frustration is concentrated in this region. Detailed comparison of the pentameric helical domains of the A subunits and the helices formed by the same amino acids in the C and D subunits that occupy the interface at the flat quasi-2-fold axes (Figure 1A) is informative (Figure 4). The disparity in variance values between the WT and NT capsids in these regions is so great that, when plotted over the same range, subtle differences in the local environments become all but impossible to discriminate. Hence, the models required independent re-scaling to enable gradations in the dynamics of the structural elements to be distinguished. This is emphasized by models that are color coded in different, non-overlapped ranges. The greatest variance in both the NT and WT capsids occurs at helices that form pentameric bundles (Figure 4A, B, top row), although the NT values are nearly double those of WT. Likewise, the variance values differ by a factor of two at the "flat" contact helices (Figure 4A, B, bottom row). The crystal structure provides no indication that the helical regions associated with the A and B subunits (residues 614–644) contribute to the quasi-equivalent quaternary structure, whereas the same residues that form the switch helices in subunits C and D are crucial for differentiating subunit interface interactions.

DISCUSSION

N. capensis ω virus procapsid assembly occurs in the baculovirus expression system and, presumably, also during normal infection, at approximately pH 7. All features of the procapsid derived in this study are consistent with an assembly process that acts to minimize differences in the quasi-equivalent subunits. Quasi-symmetry axes, when forced to pass through the center of the particle (Method 1), relate subunits in the procapsid with much greater fidelity than those in the capsid forms (Table 1). The exceptional uniformity of the variance among the quasi-equivalent subunits as well as within the tertiary structures of the subunits (Figure 3A) is consistent with the structural homogeneity revealed by Method 1 in the coordinate analysis. The biological challenge becomes one of assembling identical gene products into four structurally distinct environments. This is facilitated by minimizing the differences in those environments during initial assembly and probably enables the required reversibility for error correction. These properties are essential for proper assembly, but they do not confer the stability necessary to withstand harsh extracellular environments.

Late in the infection of the Lepidoptera insect gut cells by NωV, an apoptotic program is initiated with an associated reduction in pH to ~5 (Tomasicchio *et al*., 2007). Previous experiments showed

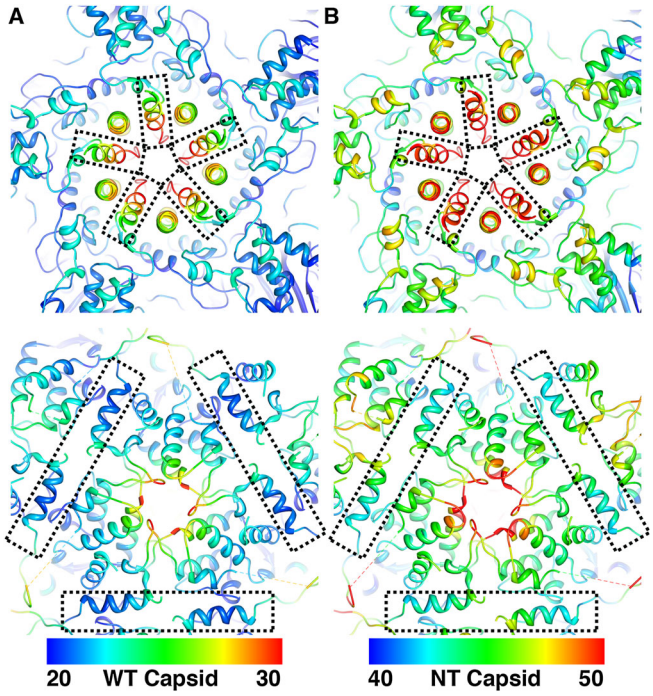

Figure 4. Increased structural fluctuations plotted as standard deviations (*i.e.*, square root of the variance) within the disordered regions of the NT capsid compared with those in the WT capsid. (A) Close-up views of the N-terminal helical bundle that surrounds the 5-fold axes (top panel) and the C-terminal switch helices that lie near the 3-fold axes (bottom) in the NT capsid with disordered regions in each highlighted by rectangles. (B) Same as panel A but for the WT capsid. These two disordered regions show increased fluctuations in the NT capsid compared with the WT capsid. Note that, unlike the global scaling employed in Figure 3, in this illustration, the range of standard deviation in each particle is mapped to a complete rainbow spectrum (blue and red represent lowest and highest standard deviation, respectively) to enhance subtle differences.

that this change in pH initiates the maturation of procapsids to capsids, which results in a dramatic size change (contracting from a diameter of 480 to 410 Å) and morphological transformation (spherical to faceted icosahedron) in the particle (Canady *et al.*, 2000). The pH-induced maturation program sends subunits on remarkably diverse trajectories that radically alter their local environments. For example, the precepts of quasi-equivalence (Caspar and Klug, 1962) predict that the A/B and C/D contacts should be closely similar, and indeed they are in the procapsid. However, in the capsid, the former pair of subunits make a dihedral angle of ~138° (bent), and the latter make an ~180° (flat) dihedral angle (Figure 1A). The different interactions at these two interfaces are readily explained by the crystal structure, where a chock-like structural element, the "switch helix", is inserted in the C/D contact that prevents the hinge motion observed in A/B. During maturation, native subunits undergo auto-proteolysis between residues 570 and 571, and this renders the chock, contributed by the C and D subunits, covalently independent but tightly associated with the particle by quaternary interactions. The N-termini of the cleaved residues in subunit A form pentameric α-helical bundles (Figure 4), which are known to be dynamically exposed on the particle surface (Domitrovic *et al.*, 2012). The half-life of the cleavage event is ~30 min, and the maturing particle gains stability that renders the transition to WT capsid irreversible. The NT capsid represents a legitimate maturation intermediate as it corresponds to the WT capsid prior to the first cleavage event.

The WT and NT capsids are morphologically indistinguishable at the spatial resolution of the cryoEM studies. However, the NT capsid shows structural variance that is two to four times larger than that in WT capsid and this is manifested primarily in the extraordinary dynamic character associated with the inner helical domains. These observations are consistent with the ability of NT capsids to reversibly expand when the pH is increased to 7.6 (Taylor *et al.*, 2002). Our analysis in this study clearly illustrates that auto-proteolysis in the C and D subunits acts to stabilize particles by allowing the helical chock to reach the ground state that is not accessible in the NT capsid. A strikingly different role of auto-proteolysis, played by A-subunit-derived γ peptides, is membrane lysis associated with translocation of the viral genome (Domitrovic *et al.*, 2012). Thus, the NωV WT capsid provides a remarkable example in which identical amino acid sequences can assume radically different roles in the virus life cycle as a consequence of quasi-equivalence.

The energetics of virus maturation provides some insights about convergent evolution. In NωV, maturation is driven by pH reduction and associated particle reorganization that creates active sites for autocatalytic cleavage and a metastable particle with an energy landscape that drives the proteolysis. As slow cleavage progresses, the particle transforms in an incremental fashion from a metastable state to a "ground state." The dsDNA bacteriophage, HK97, proceeds in a very different manner with capsid subunit tertiary structure and assembly controlled by a scaffolding domain (residues 2–103) of the subunit (Huang *et al.*, 2011). The quaternary structure of the HK97 procapsid locks the subunit tertiary structure in place and a virally encoded protease removes the scaffold domain, which then renders the particle metastable as a result of a frustrated tertiary structure (Duda *et al.*, 1995). Packaging of the dsDNA genome triggers HK97 maturation, and this occurs as a binary, large-scale expansion (Gan *et al.*, 2004). Thus, NωV moves incrementally to its ground state with a reduction in size, whereas the HK97 procapsid transitions as a two-state system to its ground state with expansion. Both processes generate energy landscapes that favor maturation but by dramatically different pathways.

CONCLUSION

We conclude that each stage of NωV assembly coordinates maturation by varying molecular recognition components. This is done by first gathering subunits with minimal variation into a fragile but stable procapsid at pH 7 and then electrostatically driving a massive subunit reorganization into a metastable intermediate at pH 5 that provides the driving force for an autocatalytic cleavage that allows the entire subunit organization to reach a ground state.

Acknowledgements

This work was supported by grants from the National Institutes of Health [RO1 GM54076 (to J.E.J.) and RO1 GM033050 (to T.S. B.)] and from the National Science Foundation [NSF 0836656 and NSF 1217867 (to P.C.D.)].

Journal of Molecular Recognition

REFERENCES

Agrawal DK, Johnson JE. 1995. Assembly of the T = 4 Nudaurelia capensis ω virus capsid protein, post-translational cleavage, and specific encapsidation of its mRNA in a baculovirus expression system. *Virology* **207**(1):89–97.

Canady MA, Tihova M, Hanzlik TN, Johnson JE, Yeager M. 2000. Large conformational changes in the maturation of a simple RNA virus, Nudaurelia capensis ω virus (NωV). *J. Mol. Biol.* **299**(3):573–584.

Caspar D, Klug A. 1962. Physical principles in the construction of regular viruses. Harbor Laboratory Press: Cold Spring, 1–24.

Domitrovic T, Matsui T, Johnson JE. 2012. Dissecting Quasi-Equivalence in Nonenveloped Viruses: Membrane Disruption Is Promoted by Lytic Peptides Released from Subunit Pentamers, Not Hexamers. *J. Virol.* **86**(18):9976–9982.

Duda RL, Hempel J, Michel H, Shabanowitz J, Hunt D, Hendrix RW. 1995. Structural transitions during bacteriophage HK97 head assembly. *J. Mol. Biol.* **247**(4):618–635.

Gan L, Conway JF, Firek BA, Cheng N, Hendrix RW, Steven AC, Johnson JE, Duda RL. 2004. Control of Crosslinking by Quaternary Structure Changes during Bacteriophage HK97 Maturation. *Mol. Cell* **14**(5):559–569.

Helgstrand C, Munshi S, Johnson JE, Liljas L. 2004. The refined structure of *Nudaurelia capensis* ω Virus reveals control elements for a *T* = 4 capsid maturation. *Virology* **318**(1):192–203.

Huang RK, Khayat R, Lee KK, Gertsman I, Duda RL, Hendrix RW, Johnson JE. 2011. The Prohead-I structure of bacteriophage HK97: implications for scaffold-mediated control of particle assembly and maturation. *J. Mol. Biol.* **408**(3):541–554.

Kleywegt GJ. 1996. Use of non-crystallographic symmetry in protein structure refinement. *Acta Crystallogr. D Biol. Crystallogr.* **52**(4): 842–857.

McLachlan AD. 1982. Rapid comparison of protein structures. *Acta Crystallogr. Sect. A: Cryst. Phy., Diffr., Theor. Gen. Crystallogr.* **38**(6):871–873.

Pettersen EF, Goddard TD, Huang CC, Couch GS, Greenblatt DM, Meng EC, Ferrin TE. 2004. UCSF Chimera—a visualization system for exploratory research and analysis. *J. Comput. Chem.* **25**(13):1605–1612.

Salzwedel K, Martin DE, Sakalian M. 2007. Maturation inhibitors: a new therapeutic class targets the virus structure. *Aids Rev* **9**(3):162–172.

Tang J, Lee KK, Bothner B, Baker TS, Yeager M, Johnson JE. 2009. Dynamics and stability in maturation of a T = 4 virus. *J. Mol. Biol* **392**(3):803.

Taylor DJ, Krishna NK, Canady MA, Schneemann A, Johnson JE. 2002. Large-scale, pH-dependent, quaternary structure changes in an RNA virus capsid are reversible in the absence of subunit autoproteolysis. *J. virol.* **76**(19):9972–9980.

Tomasicchio M, Venter PA, Gordon KH, Hanzlik TN, Dorrington RA. 2007. Induction of apoptosis in Saccharomyces cerevisiae results in the spontaneous maturation of tetravirus procapsids in vivo. *J. Gen. virol.* **88**(5):1576–1582.

Wang Q, Matsui T, Domitrovic T, Zheng Y, Doerschuk PC, Johnson JE. 2013. Dynamics in cryo EM reconstructions visualized with maximum-likelihood derived variance maps. *J. Struct. biol.* **181**(3): 195–206.

Zlotnick A, Mukhopadhyay S. 2011. Virus assembly, allostery and antivirals. *Trends in microbiol.* **19**(1):14–23.

